Modeling shear lag and demagnetization effects in magneto-electric laminate composites

Chia-Ming Chang* and Gregory P. Carman†
Mechanical and Aerospace Engineering Department, University of California, Los Angeles, 420 Westwood Plaza, Los Angeles, California 90095, USA
(Received 31 May 2007; revised manuscript received 27 August 2007; published 30 October 2007)

A quasistatic theoretical model including shear lag and demagnetizing effects is presented for predicting the magneto-electric (M-E) effects in an M-E laminate composite consisting of magnetostrictive and piezoelectric phases. Analytical solutions for strain distributions and effective M-E voltage coefficients $\bar{\alpha}$ are derived. Parametric studies are presented to evaluate the influences of material properties and geometries on strain distribution and $\bar{\alpha}$. Analytical data indicate that shear lag and demagnetization strongly influence strain distribution, and these effects cannot be ignored in predicting $\bar{\alpha}$ for most M-E laminate composites. Analytical results are also compared to experimental test data with excellent correlation for both strain distribution and $\bar{\alpha}$, i.e., less than 5% variations.

DOI: 10.1103/PhysRevB.76.134116 PACS number(s): 77.65.−j, 75.80.+q, 75.50.Gg, 75.60.−d

I. INTRODUCTION

The magnetoelectric (M-E) effect is defined as the dielectric polarization P of a material when a magnetic field H is applied, or inversely, the induced magnetization M of a material when an electric field E is applied. The M-E effect in single-phase materials was first predicted by Curie in 1894.[1] For the past two centuries, the magnetoelectric materials evolved from single phase compound[2] to particulate composites[3,4] and finally to laminate composites.[5–9] The remarkably higher M-E effect observed in laminate composites is produced by mechanically coupling continuous magnetostrictive and piezoelectric layers. For example, an M-E voltage coefficient of 22 V/cm Oe by Dong *et al.*[10] under a very low H_{bias} of 2 Oe (Ref. 11) has been reported. In order to predict the M-E effects, a precise analytical model is required. While several models for laminate M-E composite exist in the literature, these typically overpredict the experimental results significantly. This paper provides an explanation for this discrepancy and a corresponding analytical model validated with experimental results.

In 1991, Harshe *et al.*[12,13] provided an analytical foundation for M-E laminate composites. Later, Dong *et al.*[14] proposed an equivalent circuit approach for the dynamic resonance analysis. Chang and Carman[15] further considered various M-E laminate configurations (one and two dimensions) to study the influence of in-plane dimension and material properties on the M-E effect. In an attempt to explain disagreement between analysis and experiments, Bichurin *et al.*[16] proposed an interface coupling parameter k to account for sliding boundary conditions at the M-E laminate interfaces. While this provided an approach to better correlate theoretical analysis with the test data, it is unlikely that interface slip occurs at well bonded continuous interfaces. Another possible explanation which has not been considered is the shear lag effect, as originally proposed by Cox[17] in 1952 for a fiber embedded in a solid matrix. Recent development of shear lag analysis leads to precise prediction for axial stresses and displacements in an axisymmetric matrix[18] and the influences of microcracks on the axial modulus for planar problems.[19,20] Although the shear lag analysis is widely used in passive composite systems, this approach has not been widely adapted for active composite systems. In 1987, Crawley and Deluis[21] presented a modified shear lag approach to predict load transfer between piezoelectric actuators and an elastic substructure (i.e., electromechanical coupling). The corresponding stress and strain distribution in the piezoelectric laminate composite was studied and confirmed by experiments. However, shear lag has yet to be applied to an electromagnetomechanically coupled M-E composite.

In addition to shear lag, any changes of the magnetic field in the magnetostrictive layer may also influence the response of the M-E laminate composites. One well known factor is the demagnetizing field developed inside the material. The study of demagnetizing effect can be traced to the work done by Thomson,[22] Evans and Smith,[23] and Maxwell[24] in the late 19th century. Researchers typically used ellipsoids to study these materials because the ellipsoid has the only geometry that produces a uniform magnetization throughout the material. In 1942, Bozorth and Chapin[25] summarized experimental and theoretical work for demagnetizing factors in an ellipsoid. In the case of a nonellipsoid solid, the demagnetization is nonuniform and position dependent. An analytical approach for materials of a rectangular shape was developed by Joseph and Schlomann[26] in 1965. This later approach can be applied to M-E laminate composites due to the shape of a laminate.

In this paper, an analytical model is proposed to predict the response of a laminate M-E composite and is compared to experimental data. The shear lag analysis along with a demagnetization modification is incorporated to provide spatial solutions for strain, magnetic field variations, as well as effective M-E voltage coefficient $\bar{\alpha}$. The analytical study is compared to experimental tests with good agreement.

II. ANALYTICAL DEVELOPMENT

Figure 1 shows the magneto-electric (M-E) laminate composite layout studied in this paper. The M-E laminate sample consists of a piezoelectric layer on the top and bottom with a magnetostrictive layer in the middle. While the derivation is specific to this layout, the approach is valid for any lami-

 ©2007 The American Physical Society

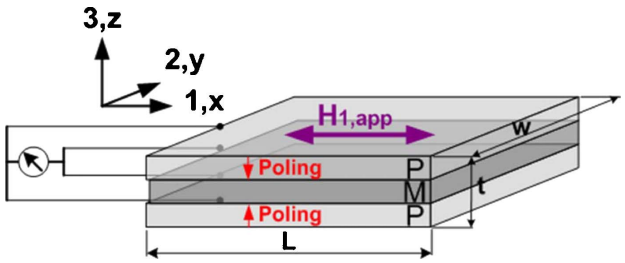

FIG. 1. (Color online) The magneto-electric (M-E) laminate composite layout.

nated M-E composite. The piezoelectric and magnetostrictive volume fractions are ${}^{p}v$ and ${}^{m}v$, respectively. The piezoelectric poling direction, defined as the 3-axis, is through the thickness and only a magnetic field is applied along the in-plane or 1 direction (i.e., absence of mechanical loads applied).

An applied magnetic field induces a deformation in the magnetostrictive layer which is transmitted to the piezoelectric layers creating a differential voltage across the thickness. The M-E voltage coefficient α is defined as $\delta E/\delta H$, where δE is the electric field in the piezoelectric phase and δH is the magnetic field applied to the sample.

The analysis assumes small deformations, linear material behavior, perfectly bonded interfaces, and open-circuit conditions for the piezoelectric layer (i.e., $D_3=0$). The open-circuit condition (i.e., absence of charge transfer) is achieved by initially shorting the electrodes prior to testing. The poled piezoelectric phase is of ∞m symmetry (i.e., transverse isotropy) about the poling axis (i.e., 3-axis) and the magnetostrictive phase is cubically symmetric (isotropic). The constitutive equations for piezoelectric and magnetostrictive materials are Piezoelectric materials:

$$
\begin{aligned}
{}^{p}\varepsilon_{ij} &= {}^{p}s_{ijkl}\,{}^{p}\sigma_{kl} + {}^{p}d_{kij}\,{}^{p}E_{k},\\
{}^{p}D_{i} &= {}^{p}d_{ikl}\,{}^{p}\sigma_{kl} + {}^{p}\in_{ij}\,{}^{p}E_{j},
\end{aligned}
\tag{1}
$$

Magnetostrictive materials:

$$
\begin{aligned}
{}^{m}\varepsilon_{ij} &= {}^{m}s_{ijkl}\,{}^{m}\sigma_{kl} + {}^{m}q_{kij}\,{}^{m}H_{k},\\
{}^{m}B_{i} &= {}^{m}q_{ikl}\,{}^{m}\sigma_{kl} + {}^{m}\mu_{ij}\,{}^{m}H_{j},
\end{aligned}
\tag{2}
$$

where ε_{ij} and σ_{kl} are strain and stress tensors, D_i and E_j are charge density and electric field, B_i and H_j are magnetic field and magnetic flux density vectors, d_{kij} and $\in_{ij}$ are piezoelectric coefficients and permittivity, q_{kij} and μ_{ij} are piezomagnetic coefficients and permeability, and s_{ijkl} is the compliance matrix. The superscripts p and m refer to either the piezoelectric phase or magnetostrictive phase, respectively.

Using traction free boundary conditions, plane stress in the thickness $(3,z)$ direction, equivalence of in-plane strains and equilibrium conditions,[12] and open-circuit conditions $(D_3=0)$, the constitutive equations [Eqs. (1) and (2)] are solved to predict the uniform (or far-field) strain and magneto-electric voltage coefficient α for an applied H_1 as shown in Eqs. (3) and (4).

$$
\begin{aligned}
{}^{p}\varepsilon_{11} = {} & \frac{{}^{p}d_{31}^{2}({}^{m}q_{11}H_1 + {}^{m}q_{12}H_1)^{m}v}{2d_{31}^{2}\,{}^{m}v - {}^{p}s_{11}\,{}^{m}v\in_{33} - {}^{p}s_{12}\,{}^{m}v\in_{33} - {}^{m}s_{11}\,{}^{p}v\in_{33} - {}^{m}s_{12}\,{}^{p}v\in_{33}} - [{}^{p}s_{12}(-{}^{p}d_{31}^{2}H_1\,{}^{m}q_{11}\,{}^{m}v^{2} + {}^{p}d_{31}^{2}H_1\,{}^{m}q_{12}\,{}^{m}v^{2}\\
& + {}^{p}s_{12}H_1\,{}^{m}q_{11}\,{}^{m}v^{2}\in_{33} - {}^{p}s_{11}H_1\,{}^{m}q_{12}\,{}^{m}v^{2}\in_{33} + {}^{m}s_{12}H_1\,{}^{m}q_{11}\,{}^{m}v\,{}^{p}v\in_{33} - {}^{m}s_{11}H_1\,{}^{m}q_{12}\,{}^{m}v\,{}^{p}v\in_{33}) - {}^{p}s_{11}({}^{p}d_{31}^{2}H_1\,{}^{m}q_{11}\,{}^{m}v^{2}\\
& - {}^{p}d_{31}^{2}H_1\,{}^{m}q_{12}\,{}^{m}v^{2} - {}^{p}s_{11}H_1\,{}^{m}q_{11}\,{}^{m}v^{2}\in_{33} + {}^{p}s_{11}H_1\,{}^{m}q_{12}\,{}^{m}v^{2}\in_{33} - {}^{m}s_{11}H_1\,{}^{m}q_{11}\,{}^{m}v\,{}^{p}v\in_{33} + {}^{m}s_{12}H_1\,{}^{m}q_{12}\,{}^{m}v\,{}^{p}v\in_{33})]/\\
& (-{}^{p}s_{11}\,{}^{m}v + {}^{p}s_{12}\,{}^{m}v - {}^{m}s_{11}\,{}^{p}v + {}^{m}s_{12}\,{}^{p}v)(2d_{31}^{2}\,{}^{m}v - {}^{p}s_{11}\,{}^{m}v\in_{33} - {}^{p}q_{12}\,{}^{m}v\in_{33} - {}^{m}s_{11}\,{}^{p}v\in_{33} - {}^{m}s_{12}\,{}^{p}v\in_{33}),
\end{aligned}
\tag{3}
$$

$$
\alpha = \frac{E_3}{H_1} = \frac{-{}^{p}d_{31}\,{}^{m}v({}^{m}q_{11} + {}^{m}q_{12})}{({}^{m}s_{11} + {}^{m}s_{12})^{p}v\in_{33} + ({}^{p}s_{11} + {}^{p}s_{12})^{m}v\in_{33} - 2({}^{p}d_{31})^{2}\,{}^{m}v}.
\tag{4}
$$

For this magnetic loading, it should be noted that ${}^{p}\varepsilon_{11} \neq {}^{p}\varepsilon_{22}$.[15] While the above is accurate in the far field, the M-E laminate composite develops nonuniform strains particularly near the free edges due to mechanical shear lag effect and demagnetization. Therefore, the strain predicted in Eq. (3) is only accurate at locations sufficiently far removed from the sample edges, and the α in Eq. (4) approaches the actual value for samples with $L \gg t$. To accurately predict the response of finite plates (i.e., Fig. 1), modifications that incorporate the influences of mechanical shear lag and demagnetization are necessary.

Figure 2 illustrates the cross-sectional diagram used in developing a one-dimensional (1D) mechanical shear lag model along the dominant direction of $H_{1,\mathrm{app}}$ (i.e., other directions are less significant). In this illustration, an elastic bonding layer of finite thickness is present between the piezoelectric and the magnetostrictive layers, and the diagram is not necessarily to scale. A differential element highlighted by the dashed block in Fig. 2 is used to derive the governing equations.

The shear lag analysis assumes pure shear in the bonding layer and pure extension in both piezoelectric and magneto-

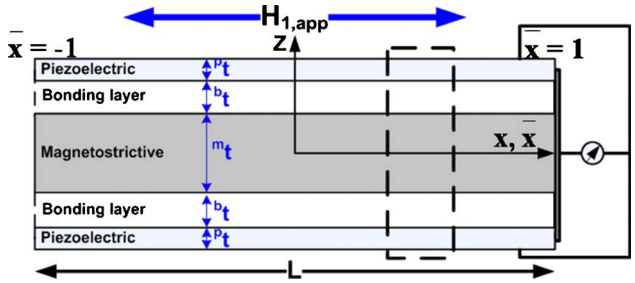

FIG. 2. (Color online) A cross-sectional diagram of M-E laminate composite with conductive bonding layers.

strictive layers. The 1D strain-displacement relationships are thus

$$ {}^{p}\varepsilon_{11} = \frac{d\,{}^{p}u_1}{dx}, \quad {}^{m}\varepsilon_{11} = \frac{d\,{}^{m}u_1}{dx}, $$

$$ {}^{b}\gamma = \frac{{}^{m}u_1 - {}^{p}u_1}{{}^{b}t}, \tag{5} $$

where ${}^{b}\gamma$ denotes the shear strain in the bonding layer, which is related to shear stress by an isotropic stress-strain relationship $\tau = {}^{b}G\,{}^{b}\gamma$. With the pure extension assumption as illustrated in the free body diagram of Fig. 3, the force equilibrium equations for the representative element are given by

$$ \frac{d\,{}^{p}\sigma_{11}}{dx} + \frac{\tau}{{}^{p}t} = 0, $$

$$ \frac{d\,{}^{m}\sigma_{11}}{dx} - \frac{2\tau}{{}^{m}t} = 0. \tag{6} $$

Using the constitutive equations [Eqs. (1) and (2)], the bonding stress-strain relations, strain-displacement equations [Eq. (5)], and the equilibrium equations [Eq. (6)], along with the open-circuit condition from a globally average perspective $D_3 = 0$, two coupled second-order M-E strain differential equations can be derived and further reduced to a pair of fourth-order differential equations as a function of strains,

$$ {}^{m}\varepsilon_{11}''' - \Gamma^2\,{}^{m}\varepsilon_{11}'' = 0, \quad {}^{p}\varepsilon_{11}''' - \Gamma^2\,{}^{p}\varepsilon_{11}'' = 0, \quad \Gamma^2 = \frac{\bar{G}\theta_b}{\bar{t}^2}\left(\frac{\Psi + 2K}{K\Psi}\right), \tag{7} $$

where the prime quantities represent differentiation with respect to a nondimensional coordinate $\bar{x} \equiv x/(L/2)$. The Γ is the shear lag parameter containing nondimensional parameters of $\bar{G} \equiv G/{}^{p}E_{11}$, piezoelectric modulus $K \equiv \in_{33}/(\in_{33} - {}^{p}E_{11}\,{}^{p}d_{31}^2)$, $\theta_b \equiv {}^{b}t/{}^{p}t$, $\bar{t} \equiv {}^{p}t/(L/2)$, and stiffness ratio $\Psi \equiv {}^{m}t_{11}\,{}^{m}t/{}^{p}E_{11}\,{}^{p}t$. In deriving Eq. (7), the piezoelectric and magnetostrictive strain distributions are coupled in the following manner with four unknown constants C_1, C_2, C_3, and C_4:

$$ \begin{bmatrix} {}^{p}\varepsilon_{11} \\ {}^{m}\varepsilon_{11} \end{bmatrix} = \begin{bmatrix} 1 \\ 1 \end{bmatrix} C_1 + \begin{bmatrix} 1 \\ 1 \end{bmatrix} C_2\bar{x} + \begin{bmatrix} -\Psi \\ \alpha K \\ 1 \end{bmatrix} C_3 \sinh\Gamma\bar{x} + \begin{bmatrix} -\Psi \\ \alpha K \\ 1 \end{bmatrix} C_4 \cosh\Gamma\bar{x}. \tag{8} $$

For the M-E laminate composite, the traction free boundary conditions are ${}^{m}\sigma_{11} = 0$ at $\bar{x} = +1$ or -1. According to Eq. (2), this implies that ${}^{m}\varepsilon_{11}$ must be equal to the induced magnetostrictive strain ${}^{m}q_{11}H_1 \equiv \Omega$. Using this information yields the following conditions at the free ends:

$$ \begin{aligned} &\bar{x} = +1: {}^{m}\varepsilon_{11} = \Omega, \quad {}^{p}\varepsilon_{11} = {}^{p}\varepsilon_{11}^{+} \\ &\bar{x} = -1: {}^{m}\varepsilon_{11} = \Omega, \quad {}^{p}\varepsilon_{11} = {}^{p}\varepsilon_{11}^{-}, \end{aligned} \quad {}^{p}\varepsilon_{11}^{+} = {}^{p}\varepsilon_{11}^{-} \text{ for symmetry}, \tag{9} $$

where ${}^{p}\varepsilon_{11}^{+}$ and ${}^{p}\varepsilon_{11}^{-}$ are the piezoelectric strain values at the free edges $\bar{x} = +1$ and $\bar{x} = -1$, respectively. Solving Eq. (8) by applying the restriction posed in Eq. (9), the modified strain distributions in the piezoelectric and magnetostrictive layers caused by shear lag effects are

$$ \begin{aligned} {}^{p}\varepsilon_{11} = \frac{1}{\Psi + 2K}\Bigg\{ &[\Psi\Omega + K({}^{p}\varepsilon_{11}^{+} + {}^{p}\varepsilon_{11}^{-})] + \left(\frac{{}^{p}\varepsilon_{11}^{+} + {}^{p}\varepsilon_{11}^{-}}{2}\right)\bar{x} \\ &+ \Psi\left[\frac{1}{\sinh\Gamma}\left(\frac{{}^{p}\varepsilon_{11}^{+} + {}^{p}\varepsilon_{11}^{-}}{2}\right)\right]\sinh\Gamma\bar{x} \\ &+ \Psi\left[\frac{1}{\cosh\Gamma}\left(\frac{{}^{p}\varepsilon_{11}^{+} + {}^{p}\varepsilon_{11}^{-}}{2} - \Omega\right)\right]\cosh\Gamma\bar{x}\Bigg\}, \end{aligned} \tag{10} $$

$$ \begin{aligned} {}^{m}\varepsilon_{11} = \frac{1}{\Psi + 2K}\Bigg\{ &[\Psi\Omega + K({}^{p}\varepsilon_{11}^{+} + {}^{p}\varepsilon_{11}^{-})] + K({}^{p}\varepsilon_{11}^{+} + {}^{p}\varepsilon_{11}^{-})\bar{x} \\ &- \left[\frac{K}{\sinh\Gamma}({}^{p}\varepsilon_{11}^{+} + {}^{p}\varepsilon_{11}^{-})\right]\sinh\Gamma\bar{x} \\ &- \left[\frac{K}{\cosh\Gamma}\left(\frac{{}^{p}\varepsilon_{11}^{+} + {}^{p}\varepsilon_{11}^{-}}{2} - \Omega\right)\right]\cosh\Gamma\bar{x}\Bigg\}. \end{aligned} \tag{11} $$

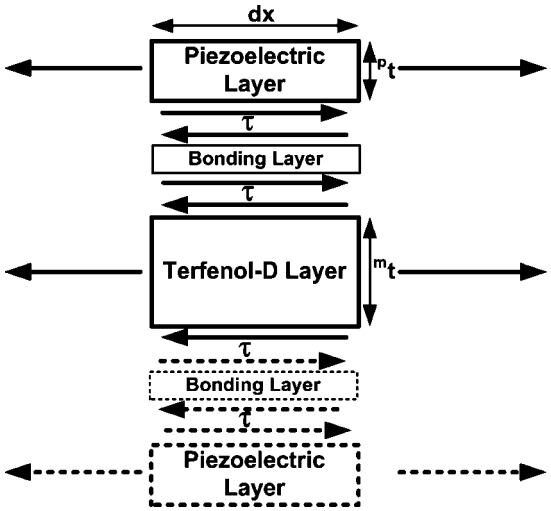

FIG. 3. Force equilibrium diagram of representative element for M-E laminate composite.

In addition to shear lag influences near the edges, demagnetizing effects also produce strain variations and influence α. For predicting the influence of demagnetization, the magnetic field can be expressed as

$$H_{1,in} = H_{1,app} - N_d M, \tag{12}$$

where, $H_{1,in}$ is the effective magnetic field with an external magnetic field of $H_{1,app}$. N_d is a demagnetizing factor which is a function of sample geometry, and M is the magnetization of the magnetostrictive layer. When demagnetization is considered, the magnetic field is altered producing changes in the magnetostrictive strain Ω. To consider demagnetization, the Ω in Eqs. (10) and (11) should be replaced by Ω_{eff}, which is related to Ω by a demagnetizing parameter Λ_d defined as follows:

$$\begin{aligned}\Omega_{eff} &\equiv {}^m q_{11} H_{1,in} = {}^m q_{11}(H_{1,app} - N_d M) \\ &= {}^m q_{11}[1 - N_d(\mu_r - 1)]H_{1,app} \\ &= [1 - N_d(\mu_r - 1)]\Omega \equiv \Lambda_d \Omega. \end{aligned} \tag{13}$$

Figure 4 shows the rectangular magnetostrictive layer used in the analytical derivation for demagnetizing effect. The nondimensional coordinate system is defined by $\bar{x} \equiv x/(L/2)$, $\bar{y} \equiv y/(w/2)$, and $\bar{z} \equiv z/({}^m t/2)$ for each axis. Under the assumption that the magnetization vector is of uniform magnitude and of the same direction with the local magnetic field, the demagnetizing factor N_d for a rectangular prism was derived by Joseph and Schlomann and presented as follows:[26]

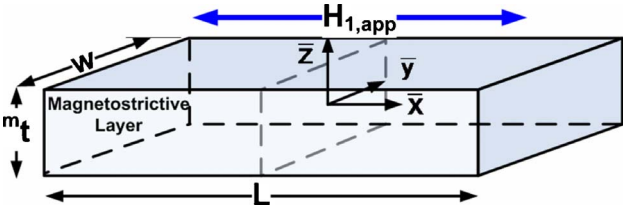

FIG. 4. (Color online) The coordinate system and the dimensions for the ferromagnetic prism.

$$\begin{aligned} N_d^{xx}(r) = (1/4\pi)\{&\cot^{-1} f(\bar{x},\bar{y},\bar{z}) + \cot^{-1} f(-\bar{x},\bar{y},\bar{z}) \\ &+ \cot^{-1} f(\bar{x},-\bar{y},\bar{z}) + \cot^{-1} f(\bar{x},\bar{y},-\bar{z}) \\ &+ \cot^{-1} f(-\bar{x},-\bar{y},\bar{z}) + \cot^{-1} f(\bar{x},-\bar{y},-\bar{z}) \\ &+ \cot^{-1} f(-\bar{x},\bar{y},-\bar{z}) + \cot^{-1} f(-\bar{x},-\bar{y},-\bar{z})\}, \end{aligned} \tag{14}$$

where

$$f(\bar{x},\bar{y},\bar{z}) = \frac{[(L/2)^2(1-\bar{x})^2 + (w/2)^2(1-\bar{y})^2 + ({}^m t/2)^2(1-\bar{z})^2]^{1/2}(L/2)(1-\bar{x})}{(w\,{}^m t/4)(1-\bar{y})(1-\bar{z})}. \tag{15}$$

As shown in Eqs. (14) and (15), the inverse trigonometric functions describe the spatially varying demagnetizing effect with maximum values at the free edges. Since the effective magnetic field $H_{1,in}$ at the free edges is trivial and the ends are traction-free, the magnetostrictive strain ${}^m\varepsilon_{11}$, as shown in Eq. (2), is equated to zero at both ends, i.e., $\bar{x} = \pm 1$. Substituting this into Eq. (11) and solving for the piezoelectric strains at the free edges yield

$$\bar{x} = \pm 1, \quad {}^p\varepsilon_{11}^{+} = {}^p\varepsilon_{11}^{-} = 0. \tag{16}$$

Using the above result, Eqs. (10) and (11) are reduced to

$$\begin{bmatrix} {}^p\varepsilon_{11} \\ {}^m\varepsilon_{11} \end{bmatrix} = \begin{bmatrix} 1 \\ 1 \end{bmatrix} \frac{\Psi\Omega_{eff}}{\Psi + 2K} + \begin{bmatrix} \dfrac{-\Psi}{2K} \\ 1 \end{bmatrix} \frac{2K\Omega_{eff}}{(\Psi + 2K)\cosh\Gamma} \cosh\Gamma\bar{x}. \tag{17}$$

This equation represents the strain distribution in an M-E laminate composite incorporating both mechanical (shear lag) and magnetic (demagnetization) influences. Using the one-dimensional constitutive equation for a piezoelectric material along with the fundamental definition for α gives

$$\alpha(\bar{x}) \equiv \frac{dE_3}{dH_1} = \left[\frac{1}{{}^p d_{31} - {}^p s_{11} \in_{33}/{}^p d_{31}}\right] \frac{d\,{}^p\varepsilon_{11}}{dH_1}. \tag{18}$$

By taking the volume integral of Eq. (18) with respect to the nondimensional coordinate system, the effective $\bar{\alpha}$ for M-E laminate composite is obtained with $\bar{V}=1$ (i.e., nondimensional coordinates),

$$\bar{\alpha} = \frac{1}{\bar{V}} \int_V \int \int \alpha(\bar{x}) d\bar{x} d\bar{y} d\bar{z}. \tag{19}$$

III. RESULTS AND DISCUSSION

In this section, the influences of shear lag effects and demagnetization influences on the piezoelectric strain distribution and magneto-electric voltage coefficient $\bar{\alpha}$ are evaluated. The material properties and geometric dimension of the sample are varied. In addition to parametric studies, the analytical model is compared with experimental measurements for strain and $\bar{\alpha}$ values. The results demonstrate excellent correlation between the analysis and test data for the M-E laminate composite.

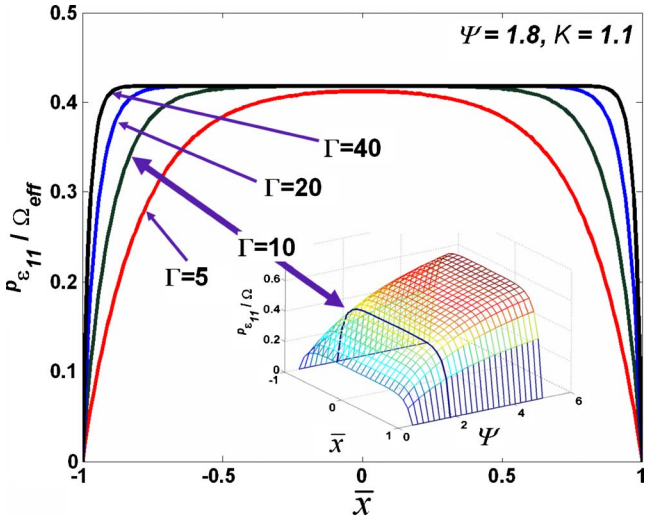

FIG. 5. (Color online) Normalized piezoelectric strain $^{p}\varepsilon_{11}/\Omega_{eff}$ for various Γ values without demagnetization at $\Psi=1.8$ and $K=1.1$.

Figure 5 plots the normalized piezoelectric strain (i.e., $^{p}\varepsilon_{11}/\Omega_{eff}$) as a function of nondimensional position $\bar{x}$ for shear lag parameters Γ equal to 5, 10, 20, and 40. The results are for a stiffness ratio of $\Psi=1.8$, a piezoelectric modulus of $K=1.1$, and demagnetizing effects are absent. The three-dimensional inset of Fig. 5 illustrates the normalized strain profile as a function of stiffness ratio Ψ and position $\bar{x}$ for a fixed $\Gamma=10$.

In general, the strains are zero at the free edges ($\bar{x}=1$ and -1) and reach the far-field strain values at the middle of the sample ($\bar{x}=0$) for all cases with the exception of $\Gamma=5$. For smaller Γ, a longer distance $\bar{x}$ is required to achieve far-field strain (i.e., compare $\Gamma=5$ to $\Gamma=40$). The Γ parameter [Eq. (7)] represents the shear transfer effectiveness, which is determined by the stiffness and thickness of the bonding layer as well as the length of the sample. As the shear modulus ^{b}G decreases, the thickness ^{b}t increases, or the sample length L becomes shorter, Γ decreases, and the shear lag influences the strain distribution profile more significantly. Based on Eq. (19), the strain variation has a direct influence on the effective M-E voltage coefficient $\bar{\alpha}$. For very large Γ, the strain distribution is relatively uniform in position [i.e., similar to Eq. (3)], producing $\bar{\alpha}$ values similar to those predicted by Eq. (4) while the $\bar{\alpha}$ values would be significantly below Eq. (4) for small Γ.

The stiffness ratio Ψ, which is defined as the product of modulus and thickness ratios of the two layers ($\Psi \equiv {}^{m}E_{11}\,{}^{m}t/{}^{p}E_{11}\,{}^{p}t$), predominately dictates the far-field strain magnitude of the piezoelectric layer. As indicated in the inset of Fig. 5, when a stiffer or thicker magnetostrictive layer (i.e., a higher Ψ) is used, a larger fraction of the magnetostrictive strain can be transferred to the piezoelectric layer and increases the far-field strain value. In the case of a very thin or soft magnetostrictive layer, Ψ approaches zero and the piezoelectric strain is trivially small.

Figure 6 shows the normalized piezoelectric strain values as a function of position $\bar{x}$ for four fixed demagnetizing parameters $\Lambda_d=0.4$, 0.6, 0.8, and 1.0 ($\Lambda_d=1$, absence of demagnetization) with a shear lag parameter of $\Gamma=10$, a stiffness parameter of $\Psi=1.8$, and a piezoelectric modulus of $K=1.1$. The contours of constant Λ_d are plotted to better illustrate the influences of demagnetizing effects on the piezoelectric strain distributions. When Λ_d decreases (i.e., demagnetization increases), far-field strain attenuation is observed and substantial strain decay occurs in $\bar{x}$ near the free ends. However, as indicated in Eqs. (13)–(15), Λ_d is a function of N_d which varies with position. The far-field values of N_d and subsequently Λ_d are nearly constant, while the near-field Λ_d values decrease as $\bar{x}$ approaches the free ends for a given specimen. Therefore, the near-field strain values actually drop more precipitously than the contours of constant Λ_d shown in Fig. 6. The N_d values are also larger for a sample with smaller aspect ratio (defined as L^2/wt). On the other hand, higher relative permeability values μ_r uniformly increase the demagnetizing effect [Eq. (13)], which attenuates the demagnetizing parameter along the whole sample. In general, samples with small aspect ratios or large permeability values have lower far-field strain values at the sample middle. At or near the ends, the Λ_d values decrease and substantially reduce the strain values in this area.

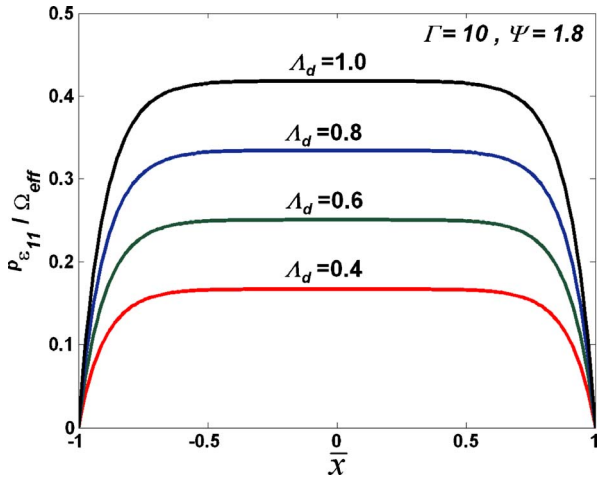

FIG. 6. (Color online) Piezoelectric strain distribution on the M-E laminate composite for various Λ_d contours at $\Gamma=10$.

To evaluate the accuracy of the analytical models, theoretical results are compared to experimental data for piezoelectric strain distribution and $\bar{\alpha}$ values. The material properties were obtained from detailed material characterization as well as commercially available property sheets. For the magnetostrictive material, the Terfenol-D composite was characterized to obtain material properties including elastic moduli ($^{m}Y_{11}$, $^{m}Y_{22}$), piezomagnetic coefficients ($^{m}q_{11}$, $^{m}q_{12}$), and relative permeability (μ_r) for various bias magnetic fields.[27] For the piezoelectric material, the piezoelectric coefficient ($^{p}d_{31}$), which relates the induced in-plane strain to the applied electric field, was measured from the slope of strain–electric-field curve under a traction-free condition. The characterization results and the other material properties along with the geometries of piezoelectric material[28] and bonding layer[29] are summarized in Table I to produce a shear lag parameter of $\Gamma=10$, a stiffness ratio of $\Psi=1.8$, and a

TABLE I. The material properties and geometric dimensions for each layer of M-E laminate composite at H_{bias}=750 Oe.

Layer/ material	s_{11} (10^{12} m^2/N)	s_{12} (10^{12} m^2/N)	${}^{m}q_{11}$ (10^{12} m/A)	${}^{m}q_{12}$ (10^{12} m/A)	${}^{p}d_{31}$ (10^{12} m/V)	${}^{b}G$ (10^{9} N/m^2)	Relative permittivity/ permeability	L (mm)	t (mm)	w (mm)
C.TED[a]	86.9	−22.6	6389	−1614			μ_r: 3.19	17.0	2.62	6.0
PZT[b]	16.1	−4.8			−230		ϵ_r: 3800	17.0	0.27	6.0
Bonding[c]	416.7					0.9		17.0	7.62×10^{-2}	6.0

[a]Reference 27.
[b]Reference 28.
[c]Reference 29.

piezoelectric modulus of K=1.1 for an M-E laminate system with a piezoelectric volume fraction ${}^{p}v$=0.17.

Figure 7 plots the piezoelectric strain distribution as a function of position ($\bar{x}$) for the experimental data[27] and theoretical results predicted using the homogeneous model [Eq. (3)], shear lag only [Eq. (17) with Λ_d=1], and shear lag plus demagnetization models [Eq. (17)]. The test is performed at an H_{bias}=750 Oe with an alternating magnetic field of H_1=125 Oe. The test data exhibit a tent-shaped distribution which is close to zero near the edges and climbs to a far-field value of 2.44×10^{-5} at the sample middle (i.e., $\bar{x}$=0), while the homogeneous solution predicts a uniform strain of 2.90×10^{-5}. This represents a 19% error between the homogeneous model and test data at the sample middle as well as significant discrepancies near the edges. For the shear lag only model, the far-field strain is 2.88×10^{-5}, which is close to the homogeneous model which exhibits a dome-shaped strain distribution. When shear lag and demagnetization are used to predict the experimental strain results, general agreement with the test data is observed throughout the specimen. Furthermore, the far-field strain of 2.57×10^{-5} is only 5% larger than the test data. Therefore, predictions that do not include shear lag and demagnetization effects substantially overpredict the test data of piezoelectric strains.

Figure 8 compares the experimental $\bar{\alpha}$ values with the various theoretical modeling results as a function of magnetic bias H_{bias} ranging from 150 to 2400 Oe. The $\bar{\alpha}$ were measured in an alternating magnetic field of H_1=125 Oe. The magnetostrictive properties, as a function of H_{bias}, were published by Chang[27] and are not presented here. All the $\bar{\alpha}$ curves increase initially with increasing H_{bias} and are followed by slow decay. The $\bar{\alpha}$ peaks are mainly attributed to the maximum piezomagnetic coefficient (${}^{m}q_{11}$) of the magnetostrictive layer at a similar H_{bias}. The largest ${}^{m}q_{11}$ is achieved in the burst region, where the magnetic domains have sufficient energy to jump from one easy axis to another as the alternating field is applied.[30] While this physical phenomenon is present in all the models, there are major differences in $\bar{\alpha}$ magnitudes for each analysis.

The homogeneous $\bar{\alpha}$ model, i.e., Eq. (3), produces the largest M-E voltage coefficient predictions and is approximately 1.63 times higher than the experimental data. The lower experimental values are due to the presence of nonuniform strain distributions shown in Fig. 8. If shear lag effect is considered, the theoretical $\bar{\alpha}$ values moderately decrease. However, the shear lag model still overpredicts experimental data by 30% as shown in Fig. 8. When shear lag and demagnetization are used [Eq. (17)], the $\bar{\alpha}$ values provide excellent correlation with the test measurements over the entire H_{bias} region studied. These data provide a convincing argument that shear lag effects and demagnetization influences must be considered for accurate $\bar{\alpha}$ predictions.

IV. CONCLUSION

A theoretical model including shear lag and demagnetizing effects has been developed for the M-E laminate com-

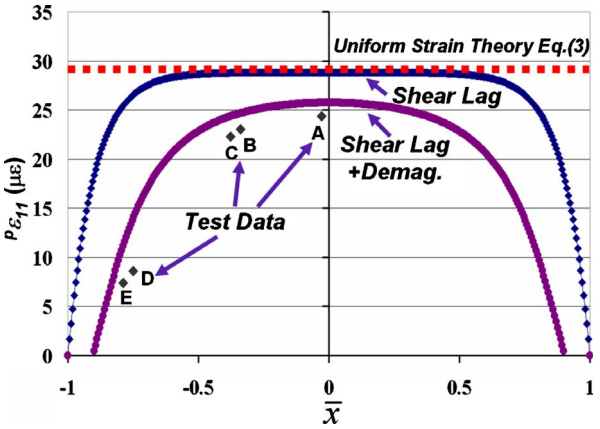

FIG. 7. (Color online) Piezoelectric strain distributions for each model and experimental data at H_{bias}=750 Oe.

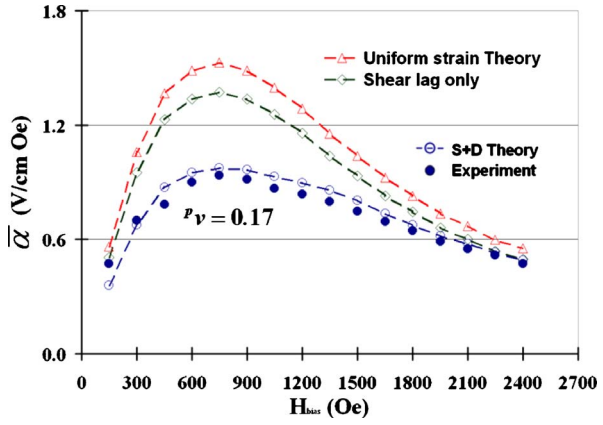

FIG. 8. (Color online) Effective magnetoelectric voltage coefficient $\bar{\alpha}$ as function of magnetic field bias for theoretical predictions and experimental data.

posite. Nondimensional shear lag parameters (Γ), stiffness ratios (Ψ), and demagnetizing parameters (Λ_d) were used to study the influences caused by material properties and sample geometries on the M-E performances. The results indicate that shear lag and demagnetizing effects cause substantial strain decay near the free ends, while demagnetizing effects decrease the far-field strain values also. By using a longer sample with a thinner and stiffer bonding layer (implying larger Γ), the shear lag effects are minimized. When a magnetostrictive layer with smaller relative permeability μ_r values and higher aspect ratios (implying larger Λ_d) are used, the demagnetization becomes less significant. Moreover, a relatively thicker and stiffer magnetostrictive layer (implying larger Ψ) increases the far-field strain values. In general, larger Γ, Ψ, and Λ_d values produce more uniform and higher strains that increase the effective $\bar{\alpha}$ values. Analytical predictions for strain and effective $\bar{\alpha}$ were also compared to experimental data. The comparison shows excellent agreement of both strain and $\bar{\alpha}$ values. However, this is only true if both shear lag and demagnetization effects are included. The results clearly demonstrate that the physical phenomenon of load transfer (i.e., shear lag) and magnetization variations (i.e., demagnetization) must be incorporated for accurate predictions in M-E laminate composite.

ACKNOWLEDGMENTS

The authors gratefully acknowledge the support provided by Air Force Office of Scientific Research and the Joint IED Defeat Organization (JIEDDO) with Byung-Lip Lee under Contract No. FA9550-07-1-0107.

*gavin@ucla.edu
†carman@seas.ucla.edu

[1] P. Curie, J. de Phys. III **3**, 393 (1894).
[2] V. J. Folen, G. T. Rado, and E. W. Stalder, Phys. Rev. Lett. **6**, 607 (1961).
[3] J. Ryu, A. V. Carazo, K. Uchino, and H. E. Kim, J. Electroceram. **7**, 17 (2001).
[4] C. W. Nan, L. Liu, N. Cai, J. Zhai, Y. Ye, Y. H. Lin, L. J. Dong, and C. X. Xiong, Appl. Phys. Lett. **81**, 3831 (2002).
[5] J. Ryu, A. V. Carazo, K. Uchino, and H. E. Kim, Jpn. J. Appl. Phys., Part 1 **40**, 4948 (2001).
[6] G. Srinivasan, E. T. Rasmussen, J. Gallegos, R. Srinivasan, Y. I. Bokhan, and V. M. Laletin, Phys. Rev. B **64**, 214408 (2001).
[7] M. I. Bichurin, V. M. Petrov, and G. Srinivasan, J. Appl. Phys. **92**, 7681 (2002).
[8] G. Srinivasan, E. T. Rasmussen, B. J. Levin, and R. Hayes, Phys. Rev. B **65**, 134402 (2002).
[9] N. Nersessian, S. W. Or, and G. P. Carman, IEEE Trans. Magn. **40**, 2646 (2004).
[10] S. X. Dong, J. Y. Zhai, J. F. Li, and D. Viehland, Appl. Phys. Lett. **89**, 122903 (2006).
[11] S. X. Dong, J. Y. Zhai, Z. Xing, J. F. Li, and D. Viehland, Appl. Phys. Lett. **91**, 022915 (2007).
[12] G. Harshe, Ph.D. thesis, Pennsylvania State University, 1991.
[13] G. Harshe, J. P. Dougherty, and R. E. Newnham, Int. J. Appl. Electromagn. Mater. **4**, 145 (1993).
[14] S. X. Dong, J. F. Li, and D. Viehland, IEEE Trans. Ultrason. Ferroelectr. Freq. Control **50**, 1253 (2003).
[15] C. M. Chang and G. P. Carman, J. Intell. Mater. Syst. Struct. (to be published).
[16] M. I. Bichurin, V. M. Petrov, and G. Srinivasan, Phys. Rev. B **68**, 054402 (2003).
[17] H. L. Cox, Br. J. Appl. Phys. **3**, 72 (1952).
[18] J. A. Nairn, Mech. Mater. **26**, 63 (1997).
[19] L. N. McCartney, J. Compos. Technol. Res. **14**, 147 (1992).
[20] J. A. Nairn and D. A. Mendels, Mech. Mater. **33**, 335 (2001).
[21] E. F. Crawley and J. Deluis, AIAA J. **25**, 1373 (1987).
[22] W. Thomson (Lord Kelvin), *Reprint of Papers on Electrostatics and Magnetism* (Macmillan, London, 1884), p. 470.
[23] F. J. Evans and A. Smith, Philos. Trans. R. Soc. London **155**, 263 (1865).
[24] J. C. Maxwell, *A Treatise on Electricity and Magnetism* (Clarendon, Oxford, 1892), Vol. 2, p. 66.
[25] R. A. Bozorth and D. M. Chapin, J. Appl. Phys. **13**, 320 (1942).
[26] R. I. Joseph and E. Schlomann, J. Appl. Phys. **36**, 1579 (1965).
[27] C. M. Chang, Ph.D. thesis, University of California, Los Angeles, 2007.
[28] Document Category No. 7, Piezo Systems, Inc., Cambridge, MA, 2006.
[29] Technical Data Sheet CF3350, Emerson & Cuming, Inc., Billerica, MA, 2007.
[30] N. Nersessian, S. W. Or, and G. P. Carman, J. Magn. Magn. Mater. **263**, 101 (2003).